Pflugers Arch - Eur J Physiol (2015) 467:1417–1430
DOI 10.1007/s00424-014-1572-5



# Characterization of the effects of $Cl^-$ channel modulators on TMEM16A and bestrophin-1 $Ca^{2+}$ activated $Cl^-$ channels

**Yani Liu · Huiran Zhang · Dongyang Huang · Jinlong Qi · Jiaxi Xu · Haixia Gao · Xiaona Du · Nikita Gamper · Hailin Zhang**

Received: 27 March 2014 / Revised: 13 June 2014 / Accepted: 30 June 2014 / Published online: 1 August 2014


**Abstract** The $Ca^{2+}$ activated $Cl^-$ channels (CaCCs) play a multitude of important physiological functions. A number of candidate proteins have been proposed to form CaCC, but only two families, the bestrophins and the TMEM16 proteins, recapitulate the properties of native CaCC in expression systems. Studies of endogenous CaCCs are hindered by the lack of specific pharmacology as most $Cl^-$ channel modulators lack selectivity and a systematic comparison of the effects of these modulators on TMEM16A and bestrophin is missing. In the present study, we studied seven $Cl^-$ channel inhibitors: niflumic acid (NFA), NPPB, flufenamic acid (FFA), DIDS, tannic acid, $CaCC_{inh}$-A01 and $T16A_{inh}$-A01 for their effects on TMEM16A and bestrophin-1 (Best1) stably expressed in CHO (Chinese hamster ovary) cells using patch clamp technique. Among seven inhibitors studied, NFA showed highest selectivity for TMEM16A ($IC_{50}$ of 7.40±0.95 μM) over Best1 ($IC_{50}$ of 102.19±15.05 μM). In contrast, DIDS displayed a reverse selectivity inhibiting Best1 with $IC_{50}$ of 3.93±0.73 μM and TMEM16A with $IC_{50}$ of 548.86± 25.57 μM. $CaCC_{inh}$-A01 was the most efficacious blocker for both TMEM16A and Best1 channels. $T16A_{inh}$-A01 partially inhibited TMEM16A currents but had no effect on Best1 currents. Tannic acid, NPPB and FFA had variable intermediate effects. Potentiation of channel activity by some of these modulators and the effects on TMEM16A deactivation kinetics were also described. Characterization of $Cl^-$ channel modulators for their effects on TMEM16A and Best1 will facilitate future studies of native CaCCs.

**Keywords** $Ca^{2+}$ activated $Cl^-$ channels (CaCCs) · TMEM16A · Bestrophin-1 · Inhibitor · CHO cells · Patch clamp

Y. Liu · H. Zhang · D. Huang · J. Qi · J. Xu · H. Gao · X. Du · N. Gamper · H. Zhang (✉)
Key Laboratory of Neural and Vascular Biology, Ministry of Education; Key Laboratory of New Drug Pharmacology and Toxicology, Hebei Province; Department of Pharmacology, Hebei Medical University, Shijizhuang, Heibei, China
e-mail: zhanghl@hebmu.edu.cn

H. Zhang
e-mail: z.hailin@yahoo.com

N. Gamper
School of Biomedical Sciences, Faculty of Biological Sciences, University of Leeds, Leeds, UK

## Introduction

Calcium activated chloride channels (CaCCs) are anionic channels with both calcium and voltage dependence. CaCCs play a variety of physiological roles in many organs and tissues, including sensory transmission, regulation of neuronal and cardiac excitability, regulation of vascular tone and transepithelial $Cl^-$ secretion (see [14] for review). The molecular identity of CaCCs remained controversial until recent years when two families of proteins were shown to function as CaCC or at least to be major components of CaCC: bestrophins and TMEM16 (anoctamin) proteins [4, 19, 20, 43, 36, 2].

Bestrophins are generally believed to form CaCC channels [27, 2, 34] and/or to regulate ion channels [35, 44]. Bestrophin-1 (Best1) is highly expressed in human basolateral membrane of retinal pigment epithelial (RPE) cells and may form the CaCC channels there [24, 37, 15]. Also in a population of sensory neurons, bestrophin has been suggested to form CaCC [2]. Moreover, hBest1 was recently found to be involved in $Ca^{2+}$ handling in endoplasmic reticulum stores [10, 46, 1]. TMEM16-proteins form a family of

transmembrane proteins with ten members some of which act as $Cl^-$ channels. Among the TMEM16 family, TMEM16A (ANO1) has been the most extensively studied; it underlies the CaCC in epithelial tissue [14, 43], neurons [18, 22, 5] and smooth muscle [23, 38]. When expressed in the expression systems, both TMEM16A and Best1 show the characteristics of endogenous CaCC: $Cl^-$ currents with $Ca^{2+}$ and voltage dependency [9, 16, 4, 36]. Both channels are sensitive to broad-spectrum $Cl^-$ channel blockers [43, 34]. The facts that (1) both TMEM16A and Best1 form functional CaCCs in expression systems; (2) both proteins are often expressed in tissues displaying native CaCC currents; (3) both channels are sensitive to conventional $Cl^-$ channel blockers make it difficult to reveal molecular identity of endogenous CaCCs.

The broad-spectrum $Cl^-$ channel blockers used in CaCC studies include niflumic acid (NFA), 4,4′-diisothiocyanatostilbene-2,2′-disulfonic acid (DIDS), 5-nitro-(3-phenylpropylamino)-benzoic acid (NPPB) and flufenamic acid (FFA). Numerous studies report that these compounds block endogenous CaCCs in *Xenopus laevis* oocytes [30, 33, 40, 41]. However, these blockers are known to be non-specific and also block other channels. For example, NFA and DIDS also block volume-regulated anion channel (VRAC) in some cell types [42, 11, 29]. NFA and FFA are shown to active $Ca^{2+}$-dependent $K^+$ channels [12, 31] whereas NFA and DIDS are found to block Kv4 channels [39] and NPPB has a blocking effect on endogenous $K^+$ currents in *Xenopus* oocytes [30, 29]. NFA, FFA and NPPB also cause an increase in intracellular $Ca^{2+}$ concentration ($[Ca^{2+}]_i$) in several cell types, which could elicit other cellular responses [30, 29]. In addition, NFA and FFA are described to modulate glutamate and glycine transporters [13]. DIDS has also been shown to increase TRPV1 current induced by capsaicin [45].

Tannic acid [26], $CaCC_{inh}$-A01 [6] and $T16A_{inh}$-A01 [25] are recently reported to inhibit CaCCs. Tannic acid

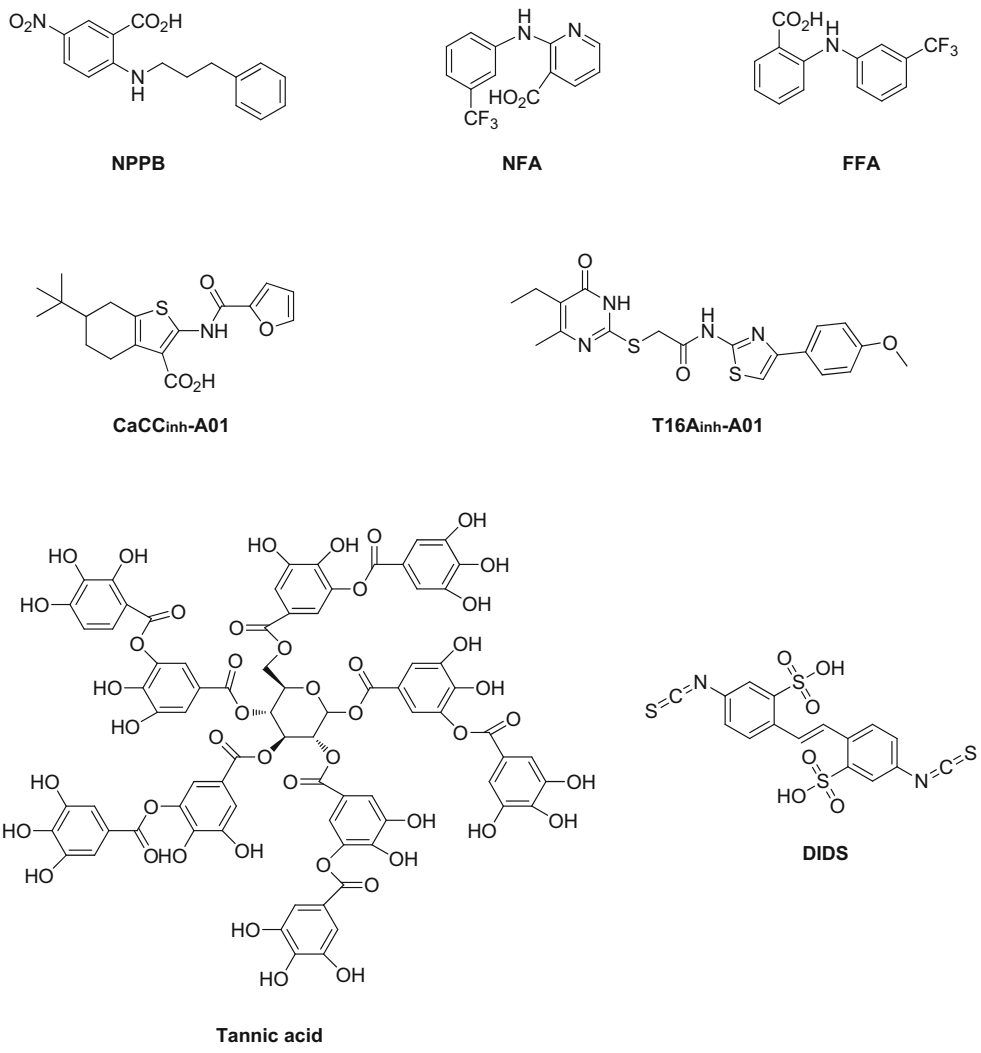


**Fig. 1** Chemical structures of CaCC inhibitors used in this study

which is present in green tea and red wine is identified as an inhibitor of TMEM16A and TMEM16B, but has little effect on CFTR $Cl^-$ conductance or on ENaC $Na^+$ conductance [26]. $CaCC_{inh}$-A01 and $T16A_{inh}$-A01 are found to inhibit TMEM16A and native CaCC. $CaCC_{inh}$-A01 is shown to target human intestinal CaCC channel directly rather than upstream signaling mechanisms, and has no effects on intracellular $Ca^{2+}$ and $Ca^{2+}$-calmodulin kinase II or CFTR [6]. $T16A_{inh}$-A01 is an aminophenylthiazole which potently inhibits TMEM16A directly without interfering with upstream processes such as agonist binding or $Ca^{2+}$ signaling [25].

Up to now, a systematic comparison study of the effects of these blockers on TMEM16A currents is lacking, and more importantly many of these compounds have not been tested for their effect on Best1

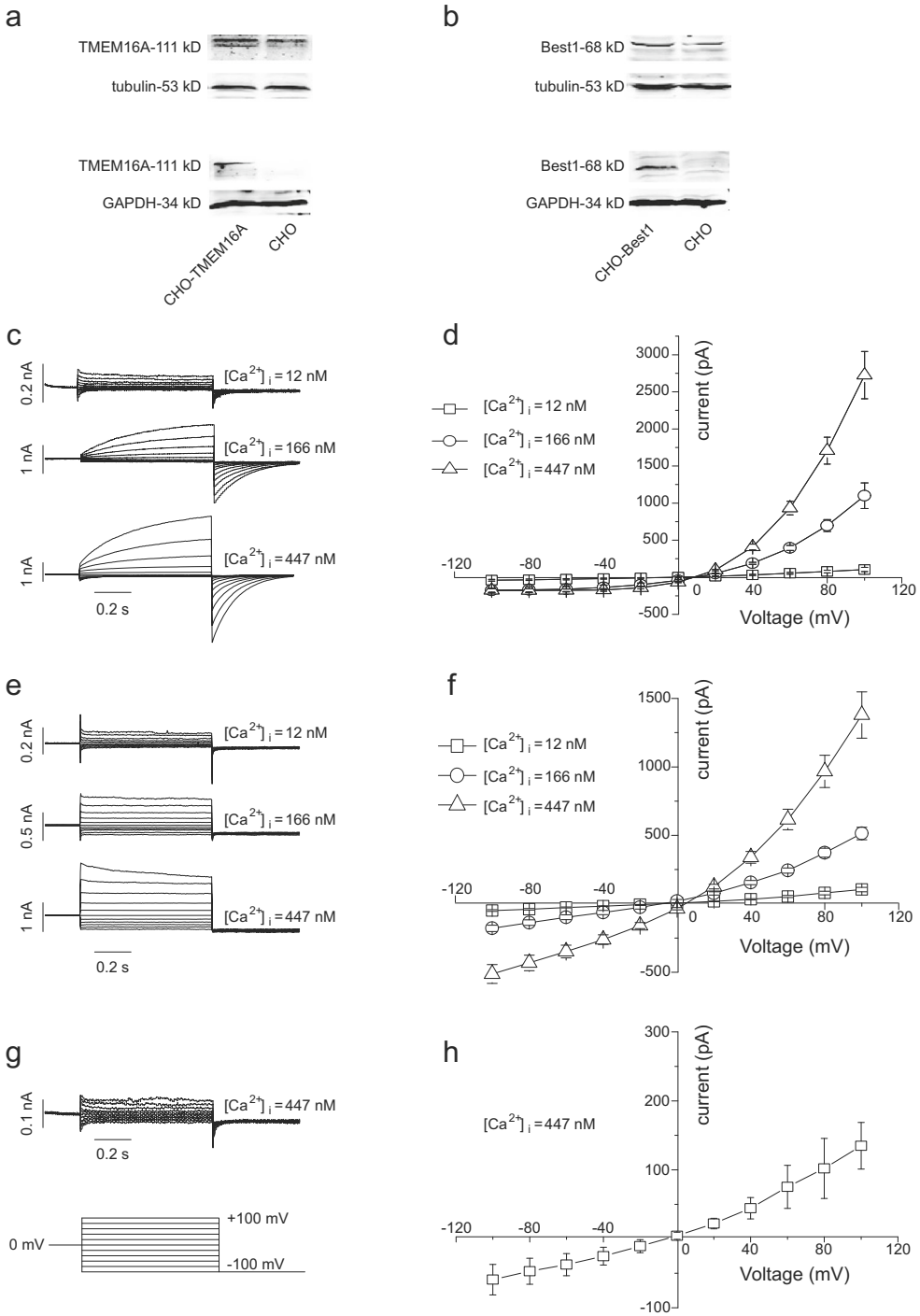


**Fig. 2** Characterization of TMEM16A and Bestrophin-1 currents in stably-transfected CHO cells. **a**, **b** Western blots results of TMEM16A and Best1 protein levels in control or stably transfected CHO cell lines. *Upper panels*: Western blots results of TMEM16A and Best1 total protein levels in control or stably transfected CHO cell lines. *Bottom panels*: Western blots results of TMEM16A and Best1 membrane protein levels in control or stably transfected CHO cell lines. **c** Whole-cell currents recorded from CHO cells expressing TMEM16A at the indicated intracellular free $Ca^{2+}$ concentrations. The currents were elicited by voltage pulses from a holding potential of 0 mV to voltages between −100 and + 100 mV in 20-mV steps followed by a step to −100 mV as indicated at the *bottom* of panel **g. d** Mean current–voltage relationships of TMEM16A at different intracellular $Ca^{2+}$ concentrations; $n$=8–15. **e** Whole-cell currents recorded from CHO cell transfected with Bestrophin-1 (*Best1*). The currents were recorded using the same protocol as used with TMEM16A. **f** Mean current–voltage relationships for the experiments shown in panel e; $n$=6–15. **g** Whole-cell currents recorded from untransfected CHO cell with 447 nM intracellular $Ca^{2+}$. **h** Mean current–voltage relationships for the experiments shown in panel **g**; $n$=5

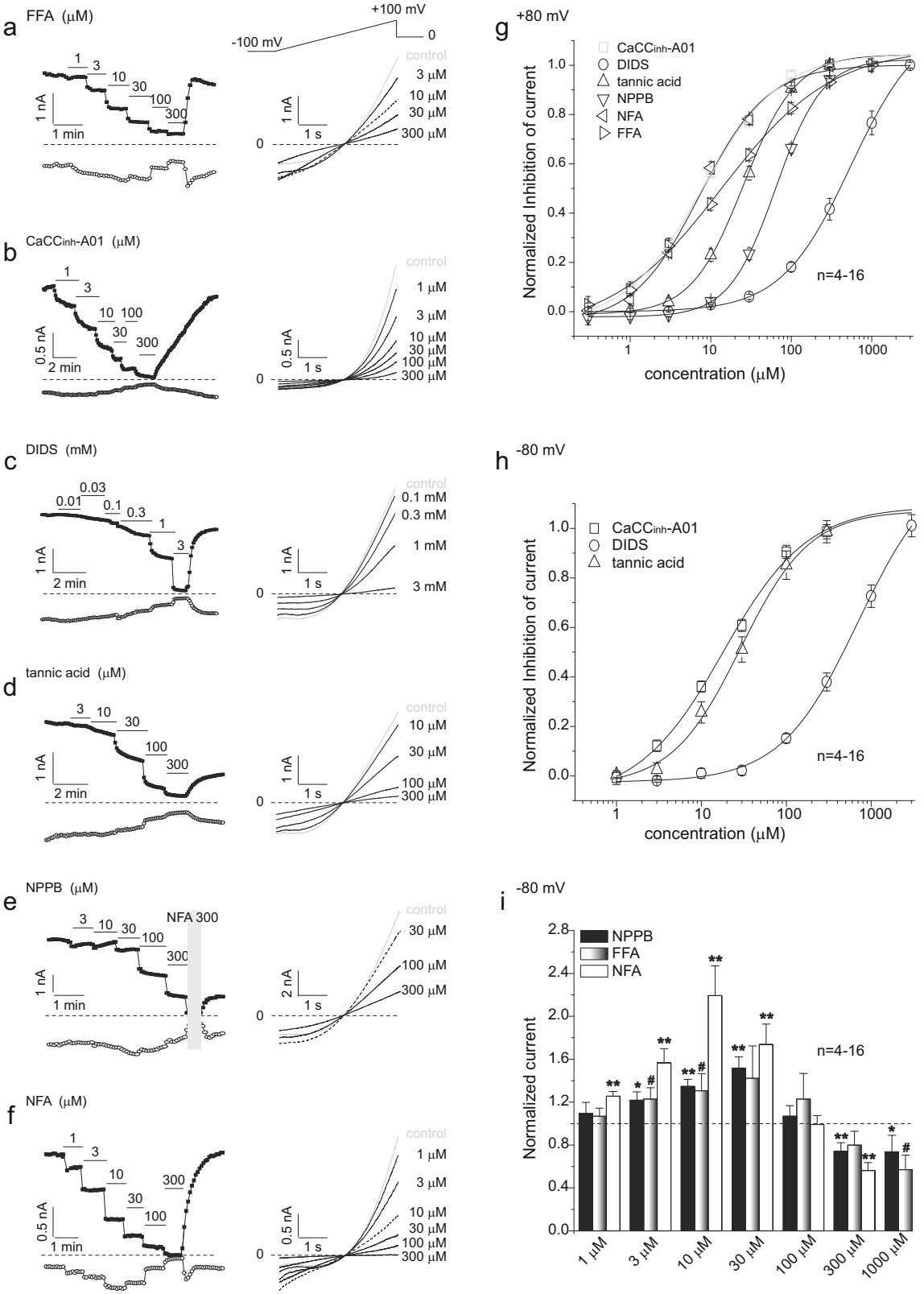


currents. In this study, we compared the efficacy and potency of seven described CaCC inhibitors (Fig. 1) on TMEM16A and Best1 currents. Profiling of different modulators of TMEM16A and Best1 will benefit our use of these modulators in studying CaCC and promote development of more specific modulators of CaCC.

◀ **Fig. 3** Effects of $Cl^-$ channel inhibitors on TMEM16A currents. Whole-cell currents of TMEM16A were induced by a voltage ramp from −100 to +100 mV. **a**–**f** *Left panels*: time courses of concentration-dependent modulation of the TMEM16A currents recorded at +80 mV (*upper line*, *black squares*) and −80 mV (*lower line*, *open circles*) with a free intracellular $Ca^{2+}$ concentration of 447 nM. The *dotted lines* indicate the zero current level. The current amplitudes were measured every 5 or 10 s. *Right panels*: the representative current traces recorded when the effect of inhibitors has stabilized. The *gray traces* are control currents in the absence of modulators. **g** Concentration–response relationships for different modulators on TMEM16A currents recorded at +80 mV. Data were fitted with logistic function. The following $IC_{50}$ values were obtained: FFA, 14.21±1.92 μM ($n$=4–12); $CaCC_{inh}$-A01, 7.84±0.62 μM ($n$=4–15); DIDS, 548.86±25.57 μM ($n$=4–16); tannic acid, 25.68±1.14 μM ($n$=6–11); NPPB, 64.14±1.56 μM ($n$=4–16); NFA, 7.40±0.95 μM ($n$=4–16). **h** Concentration–response relationships for $CaCC_{inh}$-A01 (18.39±2.34 μM, $n$=4–15), DIDS (699.37±82.81 μM, $n$=4–16) and tannic acid (29.05±4.56 μM, $n$=6–11) on the inward TMEM16A currents recorded at −80 mV. **i** Summary data for the effects of NPPB, FFA and NFA on the inward TMEM16A currents recorded at −80 mV. *$P$<0.05, **$P$<0.01 compared with basal currents in the absence of inhibitors recorded at +80 mV. $^{\#}P$<0.05, compared with basal currents in the absence of inhibitors recorded at −80 mV

## Materials and methods

### Cell culture and channel stable expression

The mouse TMEM16A cDNA clone was kindly provided by Prof. Uhtaek Oh (Seoul National University, Korea) and was subcloned to expression vector pEGFPN1. The human Best1 cDNA clone was kindly provided by Prof. Jeremy Nathans (Johns Hopkins Medical School, Baltimore,MD, USA) and was subcloned to expression vector pRK5. The human cDNA clone TMEM16A (abc) was kindly provided by Prof. Luis Galietta (Giannina Gaslini Institute, Italy) and was subcloned to expression vector pcDNA3.1. Chinese hamster ovary (CHO) cells were cultured in F-12 K with 10 % fetal calf serum and 1 % penicillin/streptomycin at 37 °C in a humidified atmosphere of 5 % $CO_2$, and were passaged every 2 days. CHO cells were transfected with above channel cDNA constructs with Lipofectamine 2000 (Invitrogen, USA) according to the manufacturer's instructions. Twenty-four hours after transfection the cells were trypsinised and plated to 9-cm Petri dishes in media supplemented with the selection factor G418 (1,000 μg/ml) for 14 days with the medium being replaced every 3–5 days. The colonies were selected and transferred to a 24-well plate, cultured and the CHO cells stably expressing TMEM16A or Best1 were identified by Western blots and patch clamp technique. Stably transfected CHO cells were cultured in F-12 K supplemented with 10 % fetal calf serum, 600 μg/ml G418 and 1 % penicillin/streptomycin at 37 °C, 5 % $CO_2$, and were removed from the culture flask by a 2-min digestion with 2.5 mg/ml trypsin (1:250) and plated at low density onto 13-mm-diameter glass coverslips in 24-well tissue culture plates for patch-clamp analysis. The cells were used for recording within 48 h.

### Western blots analysis

Control and stably transfected CHO cells were harvested in lysis buffer (20 mM Tris-base, 137 mM NaCl, 10 % glycerol, 1 % Triton-X-100, 2 mM EDTA, and 1 μl/ml protease inhibitor) and lysates were centrifuged at 17,200×g for 30 min; pellets were discarded. And supernatants were further centrifuged at 100,000×$g$ for an hour to precipitate membrane proteins. Protein samples were heated to 70 °C for 10 min in sodium dodecyl sulfate polyacrylamide gel electrophoresis (SDS–PAGE) loading buffer and separated on a 10 % polyacrylamide gel. The separated proteins were transferred at 30 V to nitrocellulose membrane (Millipore, USA) overnight at 4 °C. After blocking the membrane in TBS containing 5 % non-fat milk, the blots were incubated with primary antibodies at RT for 4–6 h. Antibody dilutions were as follows: polyclonal anti-TMEM16A, 1:500 (rabbit; Aviva System Biology, USA); polyclonal anti-bestrophin, 1:500 (rabbit; Abcam, UK); monoclonal anti-β-tubulin III, 1:500 (mouse; Sigma, USA); monoclonal anti-GAPDH 1:500 (mouse; Abcam, UK). After incubation with primary antibodies, membranes were rinsed with TBST (150 mM NaCl, 20 mM Tris-base, 0.05 % Tween-20) three times for 10 min and then incubated with secondary antibodies conjugated with IRDye700DX and

**Table 1** Effects of different inhibitors on TMEM16A and Best1 currents measured at +80 mV

| | TMEM16A | | Bestrophin1 | |
|---|---|---|---|---|
| | $E_{max}$ (% inhibition) | $IC_{50}$ (μM) | $E_{max}$ (% inhibition) | $IC_{50}$ (μM) |
| NFA | 93.65±0.79 (300 μM) | 7.40±0.95 | 87.62±2.47 (3 mM) | 102.19±15.05 |
| NPPB | 80.99±2.6 (1 mM) | 64.14±1.56 | 90.21±1.49 (300 μM) | 20.76±1.20 |
| DIDS | 93.01±1.15 (3 mM) | 548.86±25.57 | 82.57±2.34 (300 μM) | 3.93±0.73 |
| Tannic acid | 92.96±0.63 (300 μM) | 25.68±1.14 | 89.69±2.05 (300 μM) | 14.84±0.86 |
| $CaCC_{inh}$-A01 | 90.67±1.15 (300 μM) | 7.84±0.62 | 90.21±2.4 (300 μM) | 7.15±0.65 |
| FFA | 93.67±0.25 (1 mM) | 14.21±1.92 | 94.54±0.97 (1 mM) | 63.64±4.0 |
| $T16A_{inh}$-A01 | 28.74±2.19 (3 μM) | 0.31±0.59 | N/A | N/A |

All values are means±SEM ($n$=4–16)

*N/A* no activity

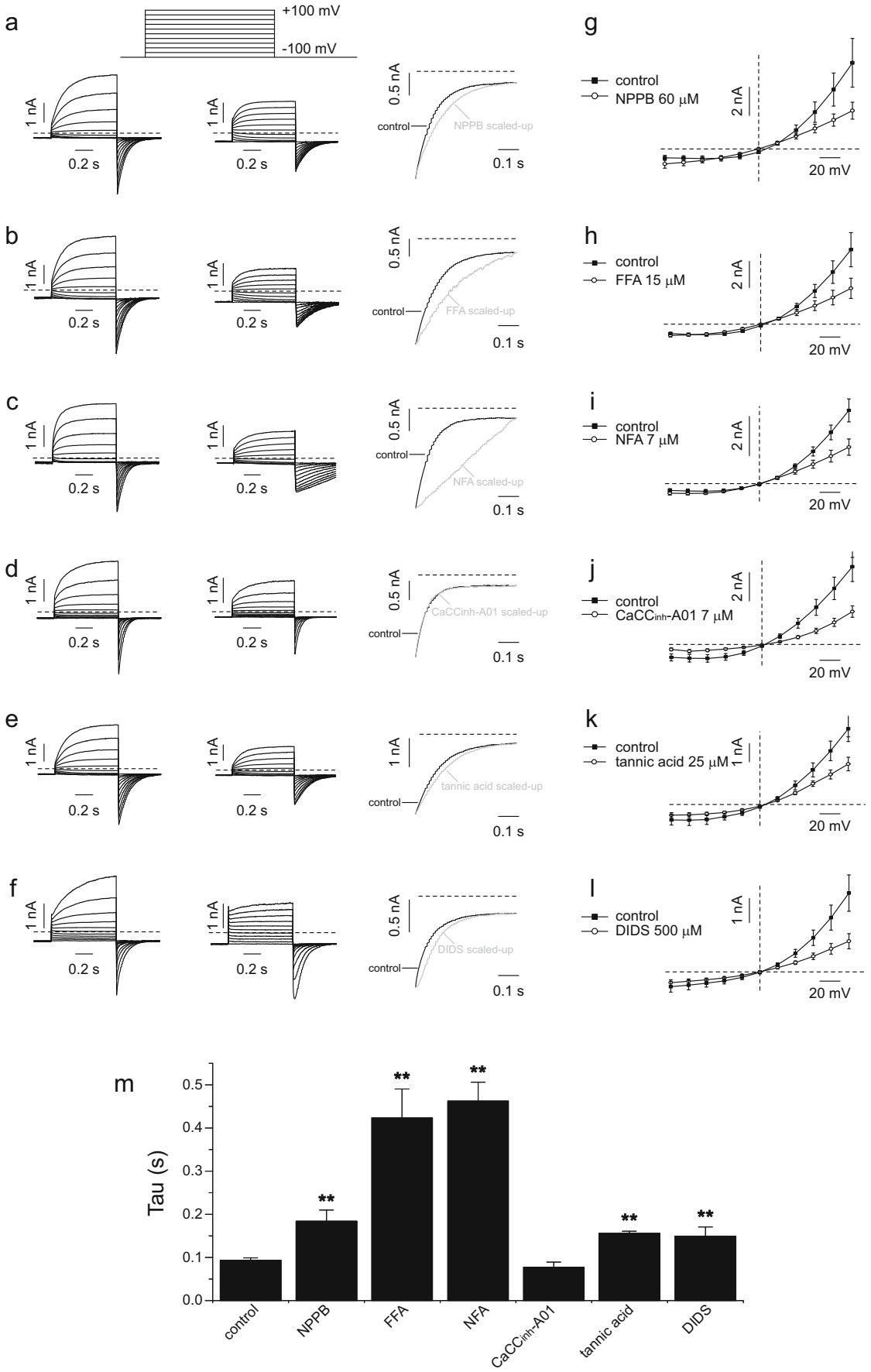
a
+100 mV
-100 mV
1 nA
0.2 s
0.5 nA
control
NPPB scaled-up
0.1 s
g
control
NPPB 60 μM
2 nA
20 mV
b
FFA scaled-up
FFA 15 μM
c
NFA scaled-up
NFA 7 μM
d
CaCCinh-A01 scaled-up
CaCCinh-A01 7 μM
e
tannic acid scaled-up
tannic acid 25 μM
f
DIDS scaled-up
DIDS 500 μM
m
Tau (s)
0.0
0.1
0.2
0.3
0.4
0.5
**
control
NPPB
FFA
NFA
CaCCinh-A01
tannic acid
DIDS

◀ **Fig. 4** Effects of $Cl^-$ channel inhibitors on steady-state TMEM16A currents and channel deactivation. **a**–**f** The cells were clamped from the holding potential of −100 mV to voltages between −100 and +100 mV in 20-mV steps followed by a step to −100 mV (voltage protocol is depicted above traces in **a**). The *dotted lines* indicate the zero current level. *Left panels*: whole cell currents recorded from CHO cells transfected with TMEM16A with a free intracellular $Ca^{2+}$ concentration of 447 nM. *Middle panels*: TMEM16A currents when the indicated inhibitors were applied. *Right panels*: effects of CaCC blockers on the deactivation kinetics of TMEM16A currents from +80 to −100 mV. The *gray line* shows the deactivating currents in the presence of the blockers, which were scaled up to match the amplitude of the deactivating currents in the absence of the blockers. **g**–**l** Current–voltage relationships of TMEM16A currents in the absence or presence of the blockers; $n$=4–6. **m** Summary of effects of CaCC blockers on the time constants of TMEM16A deactivating currents. $^{**}P<0.01$ compared with control in the absence of blockers; $n$=4–7

IRDye800CW (1:4,000 and 1:3,000, respectively; Rockland, USA) at room temperature for 1–2 h. Membranes were washed twice with TBST for 2×10 min and once with TBS for 10 min. Protein bands were detected and quantified on an Odyssey two-color infrared imaging system (LI-COR Biosciences, USA).

### Electrophysiology

TMEM16A and Best1 currents in CHO cells were recorded using whole-cell recording technique with an EPC 10 amplifier (HEKA Electronic, Germany) and PULSE software (HEKA). The acquisition rate was 10 kHz and signals were filtered at 2.5 kHz. Patch electrodes were pulled with a horizontal micropipette puller (P-97, Sutter Instruments, USA) and fire polished. The recording electrodes had a resistance of 2–4 MΩ when filled with internal solution of composition (mM): 130 CsCl, 10 EGTA, 1 $MgCl_2$, 10 HEPES and different concentrations of $CaCl_2$ to obtain the desired free $Ca^{2+}$ concentration (1 mM for 12 nM, 6 mM for 166 nM and 8 mM for 447 nM). On a day of the recording the intracellular solution was supplemented with ATP (to final concentration of 2 mM) and pH was adjusted to 7.3 with CsOH. Free $Ca^{2+}$ concentration was calculated using the Webmaxc software (Stanford; http://www.stanford.edu/~cpatton/webmaxc/webmaxcS.htm). The bath solution contained (in mM): 140 NMDG, 1 $CaCl_2$, 1 $MgCl_2$, 10 glucose, 10 HEPES and pH 7.4 adjusted with HCl. All recordings were performed at room temperature.

### Chemicals

NFA, DIDS, NPPB, $T16A_{inh}$-A01, tannic acid and FFA were purchased from Sigma (St Louis, MO, USA). Digallic acid was purchased from TRC (Toronto, Canada). $CaCC_{inh}$-A01 was synthesized in-house. The purity of $CaCC_{inh}$-A01 (>99.9 %) was determined by infrared nuclear MR and high-resolution mass spectrometry. These compounds were dissolved in DMSO to yield stock solutions of 100 mM. The stock solutions were kept at −20 °C. Stock solutions were diluted to final concentrations in bath solution. The vehicle at the final concentration did not affect the currents measured. All drug solutions were freshly made before each experiment and kept away from light.

### Data analysis and statistics

Results were expressed as means±SEM. Student's test (unpaired) was used to assess statistical significance. $P<0.05$ was considered significant. Concentration–response curves were fitted with the logistic equation: $y=A_2+(A_1-A_2)/(1+(x/x_0)^p)$; where $y$ is the response; $A_1$ and $A_2$ are the maximum and minimum response, respectively; $x$ is the drug concentration; and $p$ is the Hill coefficient. One-way ANOVA test was used to assess statistical comparison of $IC_{50}$s data. To analyze the kinetics of TMEM16A current deactivation, the tail currents deactivating from +80 to –100 mV were used to obtain the time constants. The deactivation traces were fitted to a single exponential function: $I=A\times[1-\exp(-t/\tau)]+I_0$, where $I$ is the current, $I_0$ is the steady-state amplitude of the current at the end of the holding potential of −100 mV, $A$ is the difference between the peak and steady-state current amplitudes, $t$ is time, and $\tau$ is the time constant.

## Results

### Characterization of TMEM16A and bestrophin-1 currents stably expressed in CHO cells

All experiments were performed using CHO cells that were stably transfected with mouse TMEM16A and human Best1 (see Materials and methods). Figure 2a and b shows the Western blot results of TMEM16A and Best1 protein expression. Bands corresponding to TMEM16A and Best1 were detected in both transfected and control CHO cultures, indicating possible endogenous expression of TMEM16A and Best1 in these cells. Overexpression of TMEM16A and Best1 greatly increased corresponding protein expression level (Fig. 2a and b, upper panels). However, Western blot analysis using the membrane protein indicated that levels of both TMEM16A and Best1 at the cell membranes of untransfected CHO cells were barely detectable while strong bands were detected in TMEM16A- and Best1-transfected cells (Fig. 2a and b, bottom panels). TMEM16A and Best1 currents were recorded by using the whole-cell patch-clamp technique. The cells were clamped from the holding potential of 0 mV to voltages between −100 and +100 mV in 20 mV steps followed by a step to −100 mV. TMEM16A currents were first characterized. CHO cells with stable expression of

TMEM16A manifested membrane currents with typical voltage and intracellular $Ca^{2+}$ dependence, and slow activation at high depolarizing voltages (Fig. 2c and d) [36]. The steady-state current–voltage relationship showed a strong outward

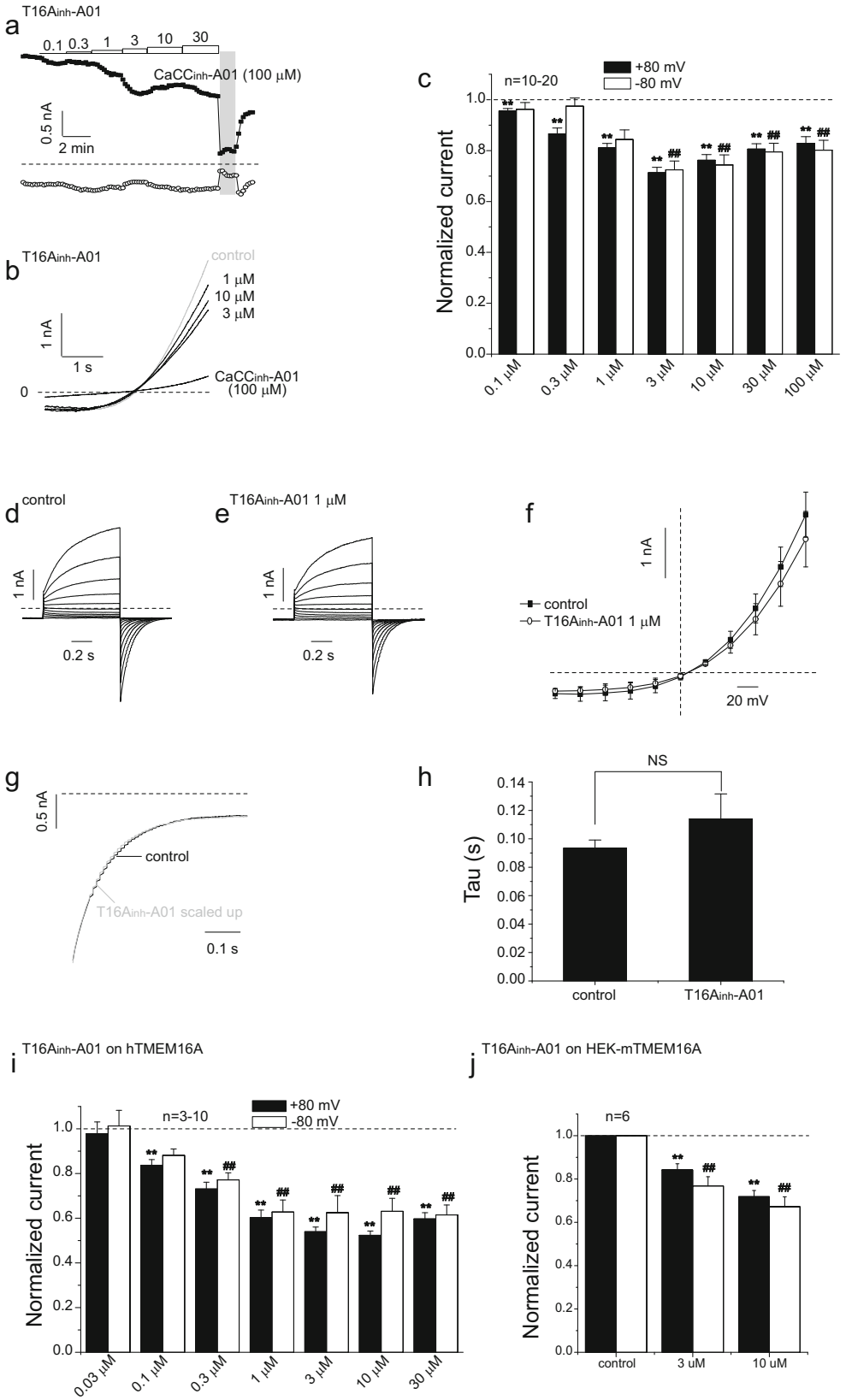

rectification in a 447 nM free intracellular $Ca^{2+}$ concentration (Fig. 2c and d). For a comparison, Best1 currents were recorded in same conditions. The CHO cells with stable expression of Best1 also presented currents with voltage and $Ca^{2+}$ dependence similar to TMEM16A currents, and outward rectification. However, the activation kinetics of Best1 currents was much faster than that of TMEM16A currents (Fig. 2e and f). No significant currents were detected in CHO cells expressing Best1 or TMEM16A when intracellular $Ca^{2+}$ concentration was low (12 nM). The untransfected CHO cells showed little currents even with high (447 nM) free intracellular $Ca^{2+}$ (Fig. 2g and h). The properties of TMEM16A and Best1 currents recorded in this study were consistent with these reported before [36, 44].

## Effects of $Cl^-$ channel inhibitors on TMEM16A currents expressed in CHO cells

We first investigated six $Cl^-$ channel inhibitors for their effect on TMEM16A currents. These inhibitors were applied at increasing concentrations from 0.1 to 3,000 μM. A voltage ramp from −100 to +100 mV in 5 s was used to record the whole-cell TMEM16A currents (Fig. 3a, right top). The effects of six blockers were quantified by measuring the changes in the current amplitude at both +80 and −80 mV induced by these drugs. Figure 3a–f (left panels) shows the time courses of concentration-dependent inhibition of the TMEM16A currents by the inhibitors recorded at −80 mV (below the dotted zero current line) and +80 mV (above the dotted zero current line); the TMEM16A currents were activated with a free intracellular $Ca^{2+}$ concentration of 447 nM. The concentration dependencies of the effects of these blockers are shown in Fig. 3g and h. Among these blockers we tested, $CaCC_{inh}$-A01 and NFA showed the highest potency in inhibiting TMEM16A currents at +80 mV, with half maximal inhibition ($IC_{50}$) of 7.84±0.62 and 7.40±0.95 μM, respectively. Both inhibitors also showed high efficacy and at the maximal tested concentration (300 μM), inhibited the TMEM16A currents recorded at +80 mV by 90.67±1.15 % and 93.65±0.79 %, respectively. On the other hand, DIDS was much less potent in inhibiting TMEM16A currents, with an $IC_{50}$ of 548.86± 25.57 μM. In summary, the six tested blockers inhibited TMEM16A currents with $IC_{50}$ values in the following order: NFA (7.40±0.95 μM, $n$=4−16)~$CaCC_{inh}$-A01 (7.84± 0.62 μM, $n$=4−15)>FFA (14.21±1.92 μM, $n$=4–12)~tannic acid (25.68±1.14 μM, $n$=6−11)>NPPB (64.14±1.56 μM, $n$= 4–16)>DIDS (548.86±25.57 μM, $n$=4–16) (Fig. 3, Table 1). Despite its low potency, DIDS almost completely inhibited the TMEM16A currents (93.01±1.15 %) at the maximal tested concentration. In general, all blockers tested significantly (~80–95 %) inhibited TMEM16A currents at the maximal tested concentrations.

When we studied the modulation of the inward TMEM16A currents by the inhibitors, it gave a different picture. Three of the six inhibitors tested, NFA, NPPB and FFA, had dual effects on the inward TMEM16A currents recorded at −80 mV (Fig. 3i): they increased the inward currents at lower concentrations and inhibited the currents at higher concentrations. NFA (Fig. 3f, right, dotted line) and FFA (Fig. 3a, right, dotted line) demonstrated a maximal activation of TMEM16A at 10 μM, which increased the inward currents by 119.4± 27.7 % and 30.58±15.99 %, respectively. NPPB at the maximal activation concentration (30 μM) (Fig. 3e, right, dotted line) increased the inward currents by 51.8±10.4 %. Moreover, a transient increase of inward currents was observed before the inhibition was relieved when the inhibitors were washed out (Fig. 3a, e and f). On the other hand, the other three inhibitors, $CaCC_{inh}$-A01, tannic acid and DIDS only showed concentration-dependent inhibition of the inward TMEM16A currents recorded at −80 mV. However, these were less potent in inhibiting the inward currents than inhibiting the outward currents recorded at+80 mV, with $IC_{50}$s at −80 mV of 18.39±2.34, 29.05±4.56 and 699.37± 82.81 μM, respectively. In addition, these inhibitors were less efficacious in inhibiting inward current with maximal inhibitions of 84.49±2.88 %, 78.7±4.47 % and 73.03±4.46 %, respectively. The effects of the six inhibitors on the TMEM16A inward current are summarized in Fig. 3i.

Ramp protocol does not allow estimating the effect of the drugs on current kinetics. To investigate effects of the drugs on the TMEM16A channel kinetics and also to test effects on currents in steady-state conditions step protocol was used (from a holding potential of −100 mV to voltages between −100 mV and +100 mV in 20-mV steps followed by a step to −100 mV). For this, we tested the effects of six inhibitors with concentrations of their respective $IC_{50}$ obtained using the voltage ramp protocol (Fig. 3 and Table 1). Not surprisingly, these inhibitors at these concentrations inhibited steady-state TMEM16A currents at positive voltages by ~50 % (Fig. 4).

◀ **Fig. 5** Effects of $T16A_{inh}$-A01 on TMEM16A currents. **a** Time course for the effect of the increasing concentrations of $T16A_{inh}$-A01 on the TMEM16A currents recorded at +80 mV (*upper line*, *black squares*) and −80 mV (*lower line*, *open circles*) with a free intracellular $Ca^{2+}$ concentration of 447 nM. The TMEM16A currents were induced using the voltage ramp protocol similar to that shown in Fig. 3a. **b** Representative current traces recorded in the presence of different concentrations of $T16A_{inh}$-A01. **c** Summary of the effects of $T16A_{inh}$-A01 on TMEM16A currents. *$P$<0.05, **$P$<0.01 compared with the control currents in the absence of $T16A_{inh}$-A01 at +80 mV. $^{\#}P$<0.05, $^{\#\#}P$<0.01 compared with the control currents in the absence of $T16A_{inh}$-A01 at −80 mV; $n$=10–20. **d**–**f** Effects of $T16A_{inh}$-A01 on TMEM16A currents recorded using voltage step protocol. **g**, **h** Effects of $T16A_{inh}$-A01 on the deactivation of TMEM16A currents. **i** Summary data for the effects of $T16A_{inh}$-A01 on currents of hTMEM16A (abc) transiently overexpressed in CHO cells. **j** Summary data for the effects of $T16A_{inh}$-A01 on currents of mTMEM16A (ac) transiently overexpressed in HEK-293 cells

Interestingly, we noted that the deactivation of the TMEM16A tail currents at −100 mV was significantly slowed by all modulators but CaCCinh-A01 (Fig. 4a–c). A detailed analysis of the time constants of the deactivating tail currents showed that effects of NPPB, FFA and NFA were most significant (Fig. 4m). As we noted above, NPPB, FFA and NFA potentiated the inward TMEM16A currents, and this slowing of channel deactivation could be a related mechanism.

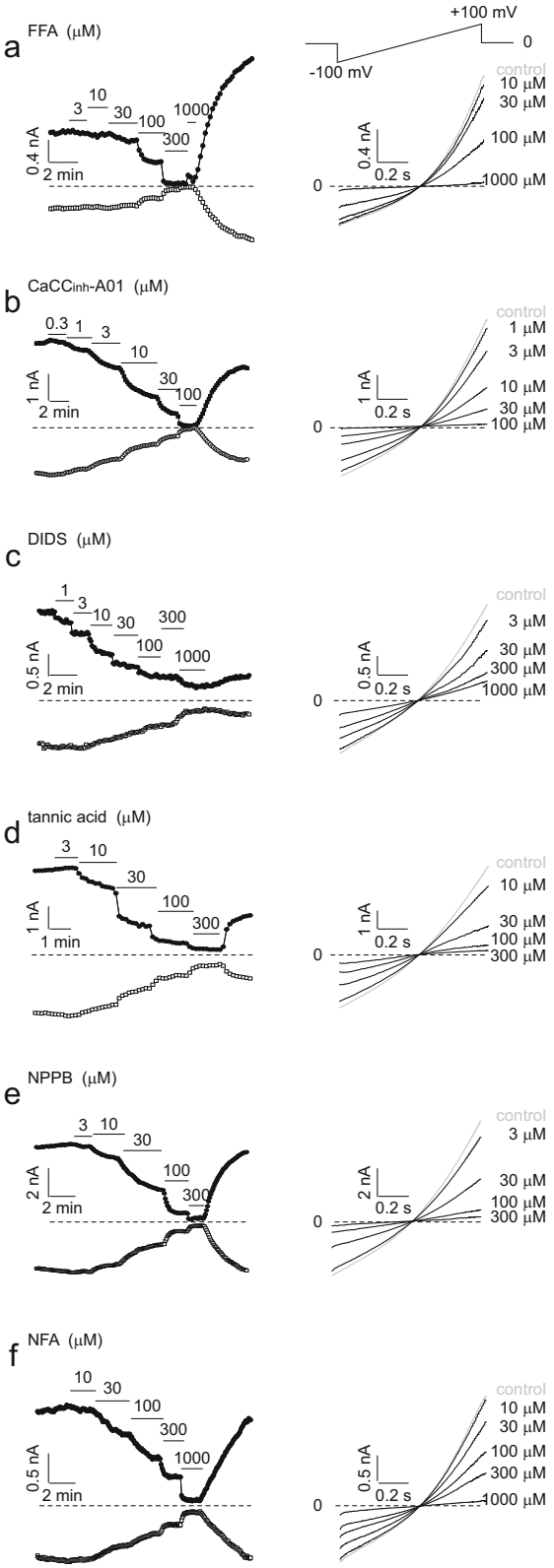


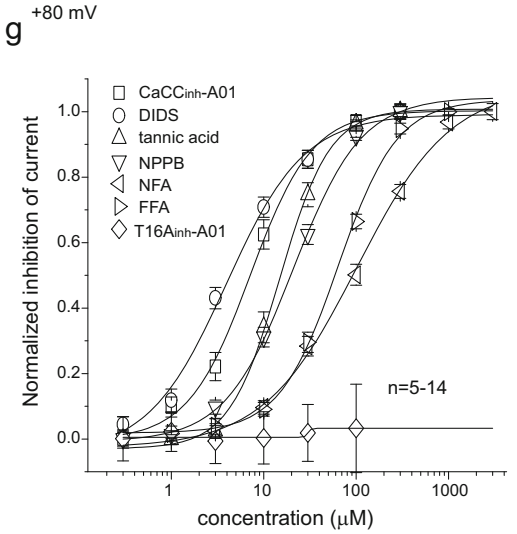


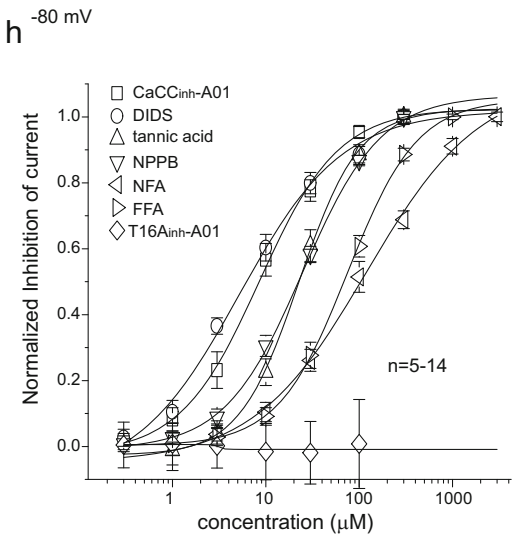

We next investigated the effect of $T16A_{inh}$-A01, a newly developed inhibitor of CaCCs [25], on TMEM16A currents. When the effect of $T16A_{inh}$-A01 was tested against TMEM16A currents recorded using the voltage ramp protocol, to our surprise, $T16A_{inh}$-A01 only showed modest inhibition of TMEM16A currents. The maximal inhibition was observed at 3 μM, with an inhibition of the outward and inward currents of 28.74±2.19 % and 27.55±3.45 % at +80 and −80 mV, respectively. It did not further inhibit the currents when the concentration was increased up to 30 μM (Fig. 5a–c). When TMEM16A currents were recorded using the step voltage protocol, similar results were observed (Fig. 5d–f). $T16A_{inh}$-A01 also did not alter the deactivation of TMEM16A currents (Fig. 5g and h). TMEM16A channel exist in several splice variants. The mouse TMEM16A used in this study does not contain segment of amino acids coded by exon 6b. To test whether the absence of exon 6b in mTMEM16A is responsible for the low sensitivity to $T16A_{inh}$-A01, we investigated the effect of $T16A_{inh}$-A01 on hTMEM16A (abc) transiently expressed in CHO cells. $T16A_{inh}$-A01 (10 μM) inhibited hTMEM16A currents measured at +80 mV by about 50 % (Fig. 5i), which is larger than the inhibition of mTMEM16A currents but still somewhat less than previously reported for hTMEM16A ac or abc isoforms [3, 25]. Finally, we also tested the effect of digallic acid, which is chemically related to tannic acid and was also reported to inhibit TMEM16A [26, 25]. However, we found that similar to $T16A_{inh}$-A01, the inhibitory effect of digallic acid at TMEM16A was weak; the compound was without an effect at concentrations below 1 mM, and at 1 mM it inhibited both mTMEM16A (ac) and hTMEM16A (abc) by 70.44±6.42 % ($n$=5) and 62.93±5.91 % ($n$=3), respectively (at +80 mV; at −80 mV inhibition was weaker; data not shown).

◀ **Fig. 6** Effects of $Cl^-$ channel inhibitors on Best1 currents. **a–f** Whole-cell currents of Best1 were induced by a voltage ramp from −100 to +100 mV. *Left panels*: time courses of concentration-dependent modulation of the Best1 currents by the increasing concentrations of blockers recorded at +80 mV (*upper line*, *black circles*) and −80 mV (*lower line*, *open circles*) with a free intracellular $Ca^{2+}$ concentration of 447 nM. The *dotted lines* indicate the zero current level. The current amplitudes were measured every 5 or 10 s. *Right panels*: representative current traces recorded when the effect of modulators has stabilized. The *gray traces* are control currents in the absence of modulators. **g** Concentration–response relationships for different inhibitors on Best1 currents recorded at +80 mV. Data were fitted with logistic function. The following $IC_{50}$ values were obtained: FFA, 63.64±4.0 μM ($n$=5–13); $CaCC_{inh}$-A01, 7.15±0.65 μM ($n$=5–14); DIDS, 3.93±0.73 μM ($n$=5–10); tannic acid, 14.84±0.86 μM ($n$=5–14); NPPB, 20.76±1.20 μM ($n$=6–14); NFA, 102.19±15.05 μM ($n$=5–14). **h** Concentration–response relationships for different inhibitors on the inward Best1 currents recorded at −80 mV. Data were fitted with logistic function. The following $IC_{50}$ values were obtained: FFA, 75.07±2.37 μM ($n$=5–13); $CaCC_{inh}$-A01, 8.53±0.78 μM ($n$=5–14); DIDS, 5.18±1.32 μM ($n$=5–10); tannic acid, 22.55±1.26 μM ($n$=5–14); NPPB, 24.76±0.72 μM ($n$=6–14); NFA, 119.76±19.15 μM ($n$=5–14)

## Effects of $Cl^-$ channel inhibitors on bestrophin-1 currents expressed in CHO cells

Next, we systematically compared all the inhibitors tested above for their effects on Best1 currents using the Best1 stably transfected CHO cells. Figure 6a–f (right panel) shows the current traces of Best1 recorded using voltage protocol shown at the top of the figure. Among the inhibitors we tested, DIDS showed the highest potency in inhibiting Best1 currents recorded at +80 mV, with an $IC_{50}$ of 3.93±0.73 μM, which was 160 folds lower than the $IC_{50}$ for TMEM16A current inhibition (Tables 1 and 2). Maximal inhibition by DIDS was 82.57±2.34 % at 300 μM (Table 1). NFA, on the other hand, was much less potent in inhibiting Best1 currents as compared to its effect on TMEM16A ($IC_{50}$s: 102.19±15.05 μM for Best1 vs. 7.40±0.95 μM for TMEM16A). At maximal concentration of 3 mM, NFA inhibited outward Best1 currents by 87.62±2.47 %. $CaCC_{inh}$-A01 inhibited Best1 currents with $IC_{50}$ of 7.15±0.65 μM and maximal inhibition of 90.21±2.4 %, which was very similar to its effects on TMEM16A currents ($IC_{50}$=7.84±0.62 μM, maximal inhibition is 90.67±1.15 %; Tables 1 and 2). Tannic acid, NPPB and FFA also inhibited Best1 currents with similar potencies as compared to their effects on TMEM16A currents (Fig. 6, Tables 1 and 2). In summary, the six tested inhibitors inhibited Best1 currents with $IC_{50}$ values in the following order: DIDS (3.93±0.73 μM, $n$=5–10)>$CaCC_{inh}$-A01 (7.15±0.65 μM, $n$=5–14)~tannic acid (14.84±0.86 μM, $n$=5–14)~NPPB (20.76±1.20 μM, $n$=6–14)>FFA (63.64±4.0 μM, $n$=5–13)>NFA (102.19±15.05 μM, $n$=5–14).

The effects of $Cl^-$ channel inhibitors on the inward currents of Best1 were also studied. Three inhibitors, NFA, NPPB and FFA, which showed dual effects of activation and inhibition of TMEM16A inward currents, did not show same pattern of effect on Best1 currents, and inhibited the inward Best1 currents recorded at −80 mV in a concentration-dependent manner. However, the potencies of the inhibitors in respect of the Best1 inward currents were slightly lower than these for the outward currents (Tables 1 and 2). Interestingly, the maximal inhibition of the inward Best1 currents by most of the inhibitors was more substantial (ranging from 93 % to 98 %), than the maximal inhibition on the outward currents (ranging from 88 % to 95 %). However, DIDS was an exception, with a 77.41±2.63 % inhibition of the inward currents as compared with an inhibition of 81.91±2.66 % of the outward currents.

Finally we tested the effect of $T16A_{inh}$-A01 and digallic acid on Best1 currents. Figure 6g and h shows that even at high concentrations, $T16A_{inh}$-A01 did not significantly affect Best1 currents recorded either at +80 mV or at −80 mV. Digallic acid (1 mM) inhibited Best1 currents by ~40 % at both voltages (data not shown).

**Table 2** Effects of different inhibitors on TMEM16A and Best1 currents measured at −80 mV

| | TMEM16A | | Bestrophin1 | |
|---|---|---|---|---|
| | $E_{max}$ (% inhibition) | $IC_{50}$ (μM) | $E_{max}$ (% inhibition) | $IC_{50}$ (μM) |
| NFA | 43.81±7.44 (300 μM) | N/A | 94.42±1.46 (3 mM) | 119.76±19.15 |
| NPPB | 26.25±15.34 (1 mM) | N/A | 94.70±0.72 (300 μM) | 24.76±1.20 |
| DIDS | 73.03±4.46 (3 mM) | 699.37±82.81 | 80.05±2.97 (300 μM) | 5.18±1.32 |
| Tannic acid | 78.7±4.47 (300 μM) | 29.05±4.56 | 92.49±2.33 (300 μM) | 22.55±1.26 |
| $CaCC_{inh}$-A01 | 84.49±2.88 (300 μM) | 18.39±2.34 | 98.45±0.77 (300 μM) | 8.53±0.78 |
| FFA | 43.04±13.7 (1 mM) | N/A | 97.04±0.81 (1 mM) | 75.07±2.37 |
| $T16A_{inh}$-A01 | 27.55±3.45 (3 μM) | N/A | N/A | N/A |

All values are means±SEM ($n$= 5–14)

*N/A* no activity

## Discussion

In this study, we first established the TMEM16A and Best1 stably transfected CHO cell lines. Although endogenous TMEM16A and Best1 proteins are expressed at low levels in untransfected CHO cells, no plasma membrane expression of TMEM16A or Best1was detected in untransfected CHO cells and no significant intracellular $Ca^{2+}$-dependent currents were detected in these cells. On the other hand, overexpression of TMEM16A and Best1 not only resulted in prominent membrane expression of these channels, but more importantly produced large intracellular $Ca^{2+}$-dependent currents with characteristics of CaCC as reported before. Thus our observed effects of the $Cl^-$ channel inhibitors should be related to the modulation of the exogenously expressed TMEM16A and Best1.

Next, we characterized the effects of seven $Cl^-$ channel inhibitors on TMEM16A and Best1 currents. The results demonstrate that $CaCC_{inh}$-A01 is the most efficacious inhibitor for both TMEM16A and Best1 currents. NFA and DIDS expressed inverse selectivity towards TMEM16A and Best1 currents, respectively. Thus, NFA inhibited TMEM16A currents with an $IC_{50}$ around 7 μM and maximal inhibition of ~94 %, as compared with an $IC_{50}$ around 100 μM and a maximal inhibition of~88 % for Best1 currents. In contrast, DIDS inhibited Best1 currents with an $IC_{50}$ around 3.5 μM, which is 160 folds lower than the $IC_{50}$ (~550 μM) for TMEM16A currents. Our work provides a direct comparison of the effects of a number of conventional and novel $Cl^-$ channel inhibitors on two CaCC channels, TMEM16A and Best1. Although effects of some of these compounds on these channels are known [17, 7, 9, 27, 37], to our knowledge no direct comparison has been carried out before, therefore our data provide clear and distinct pharmacological signatures for TMEM16A and Best1 which will inform studies of native CaCCs in the future. More importantly, the differentiating effects towards these two proposed CaCCs subunits demonstrated by some of the inhibitors will provide valuable tools to dissect their contribution to native CaCCs expressed in different cells/tissues, and to help to understand their functions. Although the molecular mechanism for the selective effects of NFA and DIDS over TMEM16A or Best1 is not clear, this finding and the differentiation of effects of other inhibitors described above provide primary information for the future development of more selective and potent $Cl^-$ channel inhibitors.

It is interesting to note that different from their effects on the outward currents, NFA, NPPB and FFA increased the inward currents of TMEM16A at low concentrations (≤30 μM) and inhibited the currents at high concentrations (≥300 μM). This is a surprising result because in previous studies, NPPB and FFA have been described as inhibitors of CaCC currents [41, 33, 40, 30]. NFA, on the other hand, has been described previously to increase the inward currents and inhibit the outward currents of the CaCC recorded from rabbit pulmonary artery myocytes [32] and rabbit coronary arterial myocytes [21]. Piper et al. [32] and Ledoux et al. [21] postulated that this dual effect of NFA could be due to the multiple binding sites in CaCC accessible by NFA. Clearly NFA, FFA and NPPB are structurally more similar when compared with other inhibitors we used (Fig. 1). This implies that a specific mechanism exists for these three inhibitors for their action on TMEM16A protein. Interestingly, NFA, FFA and NPPB markedly slowed the deactivation of TMEM16A currents (Fig. 4), proposing a mechanism for the observed potentiation of TMEM16A currents. Clearly more experiments are needed to further characterize this dual effect of the NFA, FFA and NPPB on the TMEM16A channel. No activation of inward currents of Best1 was observed for any of the inhibitors we tested. These differential effects of the inhibitors on TMEM16A and Best1 further add the value of the present study in dissecting the contribution of these two channels to endogenous CaCC and the molecular mechanisms of CaCC modulation.

The human TMEM16A has multiple isoforms which are characterized by inclusion/skipping of four segments labeled as a (116 residues), b (22 residues), c (4 residues), and d (26 residues) [4]. The biophysical properties of hTMEM16A are regulated by alternative splicing and the alternative exon 6b may play an important role in the regulation of the TMEM16A channel by $Ca^{2+}$ [8, 28]. Although $T16A_{inh}$-A01

and digallic acid have been described as a novel and high performance inhibitors of TMEM16A currents [25], in this study both compounds were found much less potent and efficacious. Thus, $T16A_{inh}$-A01 inhibited mTMEM16A (ac isoform) by about 30 % and hTMEM16A (abc isoform) by about 50 %. This is markedly lower than a value of 80 % reported in a recent patch-clamp study on heterologous hTMEM16A (ac isoform) [3] or almost complete block of hTMEM16A (abc isoform) reported by Namkung et al. [25]. It is possible that the presence of segment b can account for some of the observed difference; indeed, in both this study, and the previous investigations the (abc) isoforms appear to show some 20 % greater sensitivity to $T16A_{inh}$-A01 as compared to (ac) isoforms. Further difference can arise from the difference between human and mouse TMEM16A proteins. We tested the effect of $T16A_{inh}$-A01 with an intracellular free $Ca^{2+}$ concentration of 447 nM, which is higher than $Ca^{2+}$ concentration of 275 nM or 171 nM used in the previous studies [25, 3]. However, even at lower intracellular $Ca^{2+}$ concentration (166 nM), we still did not see significant effect of $T16A_{inh}$-A01 on mTMEM16A (ac isoform; data not shown). It is possible that the poor efficacy of $T16A_{inh}$-A01 and digallic acid on mTMEM16A expressed in CHO is related to the expression system itself and potential contamination with other TMEM16 or associated proteins. However, we tested the effect of $T16A_{inh}$-A01 on mTMEM16A overexpressed in HEK293 cells, and found $T16A_{inh}$-A01 (10 μM) inhibited TMEM16A current by 28 % at +80 mV (Fig. 5j), which was similar to the magnitude obtained in CHO expression system. It is clear though that $T16A_{inh}$-A01 does not affect Best1 currents at all.

In conclusion, the results of the present study demonstrate that the $Cl^-$ channel inhibitors inhibit TMEM16A and Best1 currents differentially, and, thus, the information provided by this study will help in further studies of CaCC.

**Acknowledgments** This work is supported by the National Natural Science Foundation of China (Grant 31270882 to HZ), the National Basic Research Program of China (Grant 2013CB531302 to HZ). We greatly appreciate the gift of mouse TMEM16A cDNA from Prof. Uhtaek Oh (Seoul National University, Korea), human Best1 cDNA from Prof. Jeremy Nathans (Johns Hopkins medical School, USA) and human TMEM16A (abc) cDNA from Prof. Luis Galietta (Giannina Gaslini Institute, Italy). We thank Yuan Wang for his kind help.

**Conflict of interest** There are no conflicts of interest.

**Author contributions** Yani Liu participated in the design of the study and carried out the experiments. Huiran Zhang and Dongyang Huang participated in the electrophysiological experiments and discussion. Jiaxi Xu participated in the cell culture and transfection experiments. Jinlong Qi synthesized $CaCC_{inh}$-A01 and contributed to experimental design and discussions; Haixia Gao and Xiaona Du participated in experimental design and discussion, Nikita Gamper contributed to data interpretation and drafting the manuscript, Hailin Zhang conceived the study, participated in its design and coordination, and drafted the manuscript.

## References

1. Barro-Soria R, Aldehni F, Almaca J, Witzgall R, Schreiber R, Kunzelmann K (2010) ER-localized bestrophin 1 activates $Ca^{2+}$-dependent ion channels TMEM16A and SK4 possibly by acting as a counterion channel. Pflugers Arch 459(3):485–497. doi:10.1007/s00424-009-0745-0
2. Boudes M, Sar C, Menigoz A, Hilaire C, Pequignot MO, Kozlenkov A, Marmorstein A, Carroll P, Valmier J, Scamps F (2009) Best1 is a gene regulated by nerve injury and required for $Ca^{2+}$-activated $Cl^-$ current expression in axotomized sensory neurons. J Neurosci 29(32):10063–10071. doi:10.1523/JNEUROSCI.1312-09.2009
3. Bradley E, Fedigan S, Webb T, Hollywood MA, Thornbury KD, McHale NG, Sergeant GP (2014) Pharmacological characterization of TMEM16A currents. Channels (Austin) 8 (3). doi:28065
4. Caputo A, Caci E, Ferrera L, Pedemonte N, Barsanti C, Sondo E, Pfeffer U, Ravazzolo R, Zegarra-Moran O, Galietta LJ (2008) TMEM16A, a membrane protein associated with calcium-dependent chloride channel activity. Science 322(5901):590–594. doi:10.1126/science.1163518
5. Cho H, Yang YD, Lee J, Lee B, Kim T, Jang Y, Back SK, Na HS, Harfe BD, Wang F, Raouf R, Wood JN, Oh U (2012) The calcium-activated chloride channel anoctamin 1 acts as a heat sensor in nociceptive neurons. Nat Neurosci 15(7):1015–1021. doi:10.1038/nn.3111
6. De La Fuente R, Namkung W, Mills A, Verkman AS (2008) Small-molecule screen identifies inhibitors of a human intestinal calcium-activated chloride channel. Mol Pharmacol 73(3):758–768. doi:10.1124/mol.107.043208
7. Dibattista M, Amjad A, Maurya DK, Sagheddu C, Montani G, Tirindelli R, Menini A (2012) Calcium-activated chloride channels in the apical region of mouse vomeronasal sensory neurons. J Gen Physiol 140(1):3–15. doi:10.1085/jgp.201210780
8. Ferrera L, Caputo A, Ubby I, Bussani E, Zegarra-Moran O, Ravazzolo R, Pagani F, Galietta LJ (2009) Regulation of TMEM16A chloride channel properties by alternative splicing. J Biol Chem 284(48):33360–33368. doi:10.1074/jbc.M109.046607
9. Francois A, Grauso M, Demondion E, Bozzolan F, Debernard S, Lucas P (2012) Bestrophin-encoded Ca(2)(+)-activated Cl(−) channels underlie a current with properties similar to the native current in the moth *Spodoptera littoralis* olfactory receptor neurons. PLoS One 7(12):e52691. doi:10.1371/journal.pone.0052691
10. Gomez NM, Tamm ER, Straubeta O (2013) Role of bestrophin-1 in store-operated calcium entry in retinal pigment epithelium. Pflugers Arch 465(4):481–495. doi:10.1007/s00424-012-1181-0
11. Greenwood IA, Large WA (1998) Properties of a $Cl^-$ current activated by cell swelling in rabbit portal vein vascular smooth muscle cells. Am J Physiol 275(5 Pt 2):H1524–H1532
12. Greenwood IA, Leblanc N (2007) Overlapping pharmacology of $Ca^{2+}$-activated $Cl^-$ and $K^+$ channels. Trends Pharmacol Sci 28(1):1–5. doi:10.1016/j.tips.2006.11.004
13. Habjan S, Vandenberg RJ (2009) Modulation of glutamate and glycine transporters by niflumic, flufenamic and mefenamic acids. Neurochem Res 34(10):1738–1747. doi:10.1007/s11064-009-9983-y
14. Hartzell C, Putzier I, Arreola J (2005) Calcium-activated chloride channels. Annu Rev Physiol 67:719–758. doi:10.1146/annurev.physiol.67.032003.154341
15. Hartzell C, Qu Z, Putzier I, Artinian L, Chien LT, Cui Y (2005) Looking chloride channels straight in the eye: bestrophins, lipofuscinosis, and retinal degeneration. Physiology (Bethesda) 20:292–302. doi:10.1152/physiol.00021.2005
16. Hartzell HC, Qu Z, Yu K, Xiao Q, Chien LT (2008) Molecular physiology of bestrophins: multifunctional membrane proteins linked to best disease and other retinopathies. Physiol Rev 88(2):639–672. doi:10.1152/physrev.00022.2007

17. Jeon JH, Paik SS, Chun MH, Oh U, Kim IB (2013) Presynaptic localization and possible function of calcium-activated chloride channel anoctamin 1 in the mammalian retina. PLoS One 8(6):e67989. doi:10.1371/journal.pone.0067989
18. Jin X, Shah S, Liu Y, Zhang H, Lees M, Fu Z, Lippiat JD, Beech DJ, Sivaprasadarao A, Baldwin SA, Gamper N (2013) Activation of the $Cl^-$ channel ANO1 by localized calcium signals in nociceptive sensory neurons requires coupling with the IP3 receptor. Sci Signal 6(290):ra73. doi:10.1126/scisignal.2004184
19. Kunzelmann K, Kongsuphol P, Aldehni F, Tian Y, Ousingsawat J, Warth R, Schreiber R (2009) Bestrophin and TMEM16-Ca(2+) activated Cl(−) channels with different functions. Cell Calcium 46(4): 233–241. doi:10.1016/j.ceca.2009.09.003
20. Kunzelmann K, Kongsuphol P, Chootip K, Toledo C, Martins JR, Almaca J, Tian Y, Witzgall R, Ousingsawat J, Schreiber R (2009) Role of the $Ca^{2+}$-activated $Cl^-$ channels bestrophin and anoctamin in epithelial cells. Biol Chem 392(1–2):125–134. doi:10.1515/BC.2011.010
21. Ledoux J, Greenwood IA, Leblanc N (2005) Dynamics of $Ca^{2+}$-dependent $Cl^-$ channel modulation by niflumic acid in rabbit coronary arterial myocytes. Mol Pharmacol 67(1):163–173. doi:10.1124/mol.104.004168
22. Liu B, Linley JE, Du X, Zhang X, Ooi L, Zhang H, Gamper N (2010) The acute nociceptive signals induced by bradykinin in rat sensory neurons are mediated by inhibition of M-type $K^+$ channels and activation of $Ca^{2+}$-activated $Cl^-$ channels. J Clin Invest 120(4): 1240–1252. doi:10.1172/JCI41084
23. Manoury B, Tamuleviciute A, Tammaro P (2010) TMEM16A/anoctamin 1 protein mediates calcium-activated chloride currents in pulmonary arterial smooth muscle cells. J Physiol 588(Pt 13):2305–2314. doi:10.1113/jphysiol.2010.189506
24. Marmorstein AD, Marmorstein LY, Rayborn M, Wang X, Hollyfield JG, Petrukhin K (2000) Bestrophin, the product of the Best vitelliform macular dystrophy gene (VMD2), localizes to the basolateral plasma membrane of the retinal pigment epithelium. Proc Natl Acad Sci U S A 97(23):12758–12763. doi:10.1073/pnas.220402097
25. Namkung W, Phuan PW, Verkman AS (2010) TMEM16A inhibitors reveal TMEM16A as a minor component of calcium-activated chloride channel conductance in airway and intestinal epithelial cells. J Biol Chem 286(3):2365–2374. doi:10.1074/jbc.M110.175109
26. Namkung W, Thiagarajah JR, Phuan PW, Verkman AS (2010) Inhibition of $Ca^{2+}$-activated $Cl^-$ channels by gallotannins as a possible molecular basis for health benefits of red wine and green tea. FASEB J 24(11):4178–4186. doi:10.1096/fj.10-160648
27. O'Driscoll KE, Leblanc N, Hatton WJ, Britton FC (2009) Functional properties of murine bestrophin 1 channel. Biochem Biophys Res Commun 384(4):476–481. doi:10.1016/j.bbrc.2009.05.008
28. O'Driscoll KE, Pipe RA, Britton FC (2011) Increased complexity of Tmem16a/Anoctamin 1 transcript alternative splicing. BMC Mol Biol 12:35. doi:10.1186/1471-2199-12-35
29. Oh SJ, Hwang SJ, Jung J, Yu K, Kim J, Choi JY, Hartzell HC, Roh EJ, Lee CJ (2013) MONNA, a potent and selective blocker for transmembrane protein with unknown function 16/anoctamin-1. Mol Pharmacol 84(5):726–735. doi:10.1124/mol.113.087502
30. Oh SJ, Park JH, Han S, Lee JK, Roh EJ, Lee CJ (2008) Development of selective blockers for Ca(2)(+)-activated Cl channel using *Xenopus laevis* oocytes with an improved drug screening strategy. Mol Brain 1:14. doi:10.1186/1756-6606-1-14
31. Ottolia M, Toro L (1994) Potentiation of large conductance KCa channels by niflumic, flufenamic, and mefenamic acids. Biophys J 67(6):2272–2279. doi:10.1016/S0006-3495(94)80712-X
32. Piper AS, Greenwood IA, Large WA (2002) Dual effect of blocking agents on $Ca^{2+}$-activated $Cl^-$ currents in rabbit pulmonary artery smooth muscle cells. J Physiol 539(Pt 1):119–131
33. Qu Z, Hartzell HC (2001) Functional geometry of the permeation pathway of $Ca^{2+}$-activated $Cl^-$ channels inferred from analysis of voltage-dependent block. J Biol Chem 276(21):18423–18429. doi:10.1074/jbc.M101264200
34. Qu Z, Wei RW, Mann W, Hartzell HC (2003) Two bestrophins cloned from *Xenopus laevis* oocytes express Ca(2+)-activated Cl(−) currents. J Biol Chem 278(49):49563–49572. doi:10.1074/jbc.M308414200
35. Rosenthal R, Bakall B, Kinnick T, Peachey N, Wimmers S, Wadelius C, Marmorstein A, Strauss O (2006) Expression of bestrophin-1, the product of the VMD2 gene, modulates voltage-dependent $Ca^{2+}$ channels in retinal pigment epithelial cells. FASEB J 20(1):178–180. doi:10.1096/fj.05-4495fje
36. Schroeder BC, Cheng T, Jan YN, Jan LY (2008) Expression cloning of TMEM16A as a calcium-activated chloride channel subunit. Cell 134(6):1019–1029. doi:10.1016/j.cell.2008.09.003
37. Sun H, Tsunenari T, Yau KW, Nathans J (2002) The vitelliform macular dystrophy protein defines a new family of chloride channels. Proc Natl Acad Sci U S A 99(6):4008–4013. doi:10.1073/pnas.052692999
38. Thomas-Gatewood C, Neeb ZP, Bulley S, Adebiyi A, Bannister JP, Leo MD, Jaggar JH (2011) TMEM16A channels generate Ca(2)(+)-activated Cl(−) currents in cerebral artery smooth muscle cells. Am J Physiol Heart Circ Physiol 301(5):H1819–H1827. doi:10.1152/ajpheart.00404.2011
39. Wang HS, Dixon JE, McKinnon D (1997) Unexpected and differential effects of $Cl^-$ channel blockers on the Kv4.3 and Kv4.2 $K^+$ channels. Implications for the study of the I(to2) current. Circ Res 81(5):711–718
40. White MM, Aylwin M (1990) Niflumic and flufenamic acids are potent reversible blockers of Ca2(+)-activated Cl− channels in Xenopus oocytes. Mol Pharmacol 37(5):720–724
41. Wu G, Hamill OP (1992) NPPB block of Ca(++)-activated Cl− currents in Xenopus oocytes. Pflugers Arch 420(2):227–229
42. Xu WX, Kim SJ, So I, Kang TM, Rhee JC, Kim KW (1997) Volume-sensitive chloride current activated by hyposmotic swelling in antral gastric myocytes of the guinea-pig. Pflugers Arch 435(1):9–19
43. Yang YD, Cho H, Koo JY, Tak MH, Cho Y, Shim WS, Park SP, Lee J, Lee B, Kim BM, Raouf R, Shin YK, Oh U (2008) TMEM16A confers receptor-activated calcium-dependent chloride conductance. Nature 455(7217):1210–1215. doi:10.1038/nature07313
44. Yu K, Xiao Q, Cui G, Lee A, Hartzell HC (2008) The best disease-linked $Cl^-$ channel hBest1 regulates Ca V 1 (L-type) $Ca^{2+}$ channels via src-homology-binding domains. J Neurosci 28(22):5660–5670. doi:10.1523/JNEUROSCI.0065-08.2008
45. Zhang X, Du XN, Zhang GH, Jia ZF, Chen XJ, Huang DY, Liu BY, Zhang HL (2012) Agonist-dependent potentiation of vanilloid receptor transient receptor potential vanilloid type 1 function by stilbene derivatives. Mol Pharmacol 81(5):689–700. doi:10.1124/mol.111.076000
46. Zhang Y, Stanton JB, Wu J, Yu K, Hartzell HC, Peachey NS, Marmorstein LY, Marmorstein AD (2010) Suppression of $Ca^{2+}$ signaling in a mouse model of Best disease. Hum Mol Genet 19(6): 1108–1118. doi:10.1093/hmg/ddp583